HHS Public Access

Author manuscript

Methods Mol Biol. Author manuscript; available in PMC 2020 September 24.

Published in final edited form as:

Methods Mol Biol. 2016 ; 1345: 251–268. doi:10.1007/978-1-4939-2978-8_16.

Computational Methods for Structural and Functional Studies of Alzheimer's Amyloid Ion Channels

Hyunbum Jang[1], **Fernando Teran Arce**[2,3], **Joon Lee**[3], **Alan L. Gillman**[2], **Srinivasan Ramachandran**[2,3], **Bruce L. Kagan**[4], **Ratnesh Lal**[2,3], **Ruth Nussinov**[1,5]

[1]Cancer and Inflammation Program, Leidos Biomedical Research, Inc., Frederick National Laboratory for Cancer Research, National Cancer Institute at Frederick, Frederick, USA

[2]Department of Bioengineering, Materials Science Program, University of California, San Diego,La Jolla,USA

[3]Department of Mechanical and Aerospace Engineering, Materials Science Program,University of California, San Diego, La Jolla, USA

[4]Department of Psychiatry, David Geffen School of Medicine, Semel Institute for Neuroscience and Human Behavior, University of California, Los Angeles, USA

[5]Department of Human Molecular Genetics and Biochemistry, Sackler School of Medicine, Tel Aviv University,Tel Aviv, Israel

Abstract

Aggregation can be studied by a range of methods, experimental and computational. Aggregates form in solution, across solid surfaces, and on and in the membrane, where they may assemble into unregulated leaking ion channels. Experimental probes of ion channel conformations and dynamics are challenging. Atomistic molecular dynamics (MD) simulations are capable of providing insight into structural details of amyloid ion channels in the membrane at a resolution not achievable experimentally. Since data suggest that late stage Alzheimer's disease involves formation of toxic ion channels, MD simulations have been used aiming to gain insight into the channel shapes, morphologies, pore dimensions, conformational heterogeneity, and activity. These can be exploited for drug discovery. Here we describe computational methods to model amyloid ion channels containing the β-sheet motif at atomic scale and to calculate toxic pore activity in the membrane.

Keywords

Amyloid channel; β-Sheet channel; Lipid bilayer; Molecular dynamics simulations; CHARMM; NAMD

1 Introduction

Alzheimer's disease (AD) is characterized by the presence of extracellular plaques, intracellular neurofibrillary tangles, and the loss of synapses and neurons in the brain of AD

patients [1]. As a subclass of fatal protein deposition diseases [2–8], termed amyloidosis, AD is caused by misfolded, water insoluble aggregates of amyloid-β (Aβ) peptides [5]. During their self-assembly into mature fibrils, Aβ peptides explore various organizations including small oligomers (globular and fibril-like) and protofibrils (straight, bent, and annular) [9, 10]. Although early studies pointed to fibrillar deposits of Aβ peptides in the extracellular plaques as directly associated with the cause of the disease [11], the current amyloid cascade hypothesis in AD points to small Aβ oligomers as the main toxic species [12–16]. However, the mechanism of the amyloid toxicity is still not entirely understood.

The interaction of Aβ with the cell membrane is a fundamental chemical feature in the mechanism of AD pathogenesis [17–19]. Upon binding to the cell membrane, Aβ undergoes conformational changes to insoluble β-sheet-rich aggregates ranging from small oligomers to fibrils [20–22]. The oligomeric Aβ aggregates are responsible for disrupting cellular function, inducing cytotoxicity [23] through ion channel formation [24]. The evidence for the presence of amyloid ion channel was first reported two decades ago, by exploiting planar lipid bilayer (PLB) measurements [25–28]. The experiments discovered that Aβ induced unregulated ionic flux across model membranes through the formation of non-gated ion channels. Subsequently, atomic force microscopy (AFM) provided the images of amyloid channels formed by Aβ peptides [12, 29] and by other disease-related amyloid species [12], suggesting that channel formation is a general feature for amyloids. The AFM images revealed that the amyloid channels exhibited various shapes from rectangular with four subunits to octahedral with eight. The heterogeneity in the Aβ channel conformations was further confirmed by recent extensive molecular dynamics (MD) simulations [30–42]. These showed that Aβ channels consisted of β-sheet-rich subunits with morphologies and dimensions in good agreement with the imaged AFM channels [12, 29]. The simulations of other amyloids and β-hairpin peptides showed that the subunit-assembly morphology is a common feature for the membrane embedded β-sheet channels [43–45].

To form an ion channel, small oligomers of Aβ insert into the membrane and assemble into common β-sheet-rich structural motifs. Recent studies indicated that small fibril-like Aβ oligomers [46] with a solvent exposed hydrophobic face [47] and parallel β-sheet structures [48] could induce neurotoxicity, providing an Aβ oligomer morphology with potential relevance to AD. These membrane-inserted small oligomers can easily align to form the toxic amyloid ion channels. While experimental tools are limited in defining the channel structure in the membrane environment, computational studies can provide their three-dimensional, atomic-level conformation. Here, we detail the computational methods of how to model β-sheet channels and to calculate pore activity in the membrane.

2 Materials: Recruiting Monomer Conformations

2.1 U-Shaped Peptides with the β-Strand-Turn-β-Strand Motif

Amyloids tend to aggregate to form a highly ordered fibrillar structure. In this organization, peptides fold into the U-shaped *β-strand-turn-β-strand* motif, which associates into stacked β-sheets with intermolecular hydrogen bonds (H-bonds). Recent computational and NMR studies defined several amyloid peptides with such U-shaped motif [49–53]. Using their reported atomic coordinates, these peptides were recruited in computational studies for the

atomistic modeling of amyloid channels in aqueous and lipid environments [30–43, 46, 54–57].

1. $A\beta_{16–35}$ peptide:The U-shaped Aβ peptide was first introduced by a computational model using molecular dynamics (MD) simulations [49]. The $A\beta_{16–35}$ peptidecontainsan intramolecular salt bridge between residues Asp23 and Lys28 near a turn at Val24-Asn27 (Fig. 1a).

2. $A\beta_{17–42}$ peptide: A combination of hydrogen/deuterium-exchange nuclear magnetic resonance (NMR) data, side-chain packing constraints from pairwise mutagenesis, solid-state NMR (ssNMR), and electron microscopy (EM) defined $A\beta_{1–42}$ fibril (pdb code: 2BEG) [50]. The $A\beta_{1–42}$ peptide provided the coordinates for residues 17–42, while the N-terminal coordinates (residues 1–16) were missing due to disorder. The $A\beta_{17–42}$ peptide has a turn at Ser26-Ile31 and the salt bridge of Asp23/Lys28 (Fig. 1b).

3. $A\beta_{9–40}$ peptide: Studies using ssNMR defined small $A\beta_{1–40}$ protofibrils (pdb codes: 2LMN and 2LMO) [51]. The N-terminal coordinates (residues 1–8) were missing due to disorder. The $A\beta_{9–40}$ peptide has a turn at Asp23-Gly29 and the same salt bridge of Asp23/Lys28 (Fig. 1c).

4. $A\beta_{11–40}$ peptide: Comprehensive ssNMR techniques defined $A\beta_{1–40}$ fibrils [52]. The N-terminal coordinates (residues 1–10) were missing due to disorder. The $A\beta_{11–40}$ peptide has a turn at Val24-Ala30, but has a shifted inter β-strand contacts within the U-shaped motif. Unlike the previous NMR models (**item 3 above**), the peptide did not contain the salt bridge of Asp23/ Lys28 (Fig. 1d).

5. The U-shaped motif is a general feature of amyloid organization. Other amyloids, such as β_2-microglobulin fragment (K3 peptide, pdb code: 2E8D) [53] (Fig. 1e) and the second WW domain of CA150 (pdb code: 2NNT) [58], also exhibit the U-shaped motif with the *β-strand-turn-β-strand* motif.

2.2 β-Hairpin Peptides

Monomeric or dimeric amyloids tend to form a β-hairpin, an aggregate intermediate that facilitates membrane insertion [46]. Conversion to the U-shaped structure in the oligomerization process with β-hairpin monomers or small oligomers followed by membrane insertion takes place in the membrane. The membrane insertion mechanism of amyloid β-hairpins is similar to that of the cytolytic cationic β-hairpins, such as protegrin-1 (PG-1) and MAX peptides. These β-hairpins are also capable of forming ion channels. [44, 45, 59].

1. PG-1 peptide: A small cationic β-hairpin peptide consisting of 18 amino acids is capable of forming β-sheet channels [44, 45]. PG-1 is an antimicrobial peptide (AMP) with a great antibiotic potency [60]. NMR determined the PG-1 β-hairpin structure in solution with the data confirming to the presence of two antiparallel β-strands linked by a β-turn and stabilized by two disulfide bonds [61–64] (Fig. 1f).

2. MAX peptides: Synthetic amphiphilic cationic peptides, MAX1 and MAX35, can form β-barrels inducing membrane leakage [59]. The MAX peptides consisting of 20 amino acids and contain alternative hydrophobic (Val or Ile) and hydrophilic (Lys) residues connected by a reciprocal turn, -V^{D}PPT-, where ^{D}P denotes the D-amino acid proline (Fig. 1g).

2.3 Lipids

To simulate amyloid channels in a membrane environment, a unit cell containing two layers of lipids is constructed. In the middle of the unit cell, simple van der Waals (vdW) spheres representing lipid headgroups are placed in two parallel planes (or membrane surfaces) separated by expected bilayer thickness [65, 66]. Dynamics are performed on the spheres with constraints on their respective planes and with the embedded channel held rigid, resulting in vdW spheres that are randomly distributed onto the planes and well packed around the channel. The lipid molecules are randomly selected from the library of pre-equilibrated states and replaced with pseudo-vdW spheres at the positions of the lipid headgroup constituting the lipid bilayer topology. Simulations employ both zwitterionic and anionic lipid bilayers with various lipids in the liquid phase. Each lipid used in the simulations exhibits different phase transitions yielding different physical properties for the cross-sectional area per lipid, A_{cross}, and headgroup distance, D_{HH}. Thus, with a proper choice for the number of lipid molecules, the optimal value of the lateral cell dimensions can be determined. The following list shows the lipid molecules used in the amyloid channel simulations.

1. DOPC: 1,2-dioleoyl-*sn-glycero*-3-phosphocholine, zwitterionic, A_{cross} = 72.4 Å^2 and D_{HH} = 36.7 Å at 30 °C [67].
2. DOPS: 1,2-dioleoyl-*sn-glycero*-3-phosphoserine, anionic, A_{cross} = 65.3 Å^2 and D_{HH} = 38.4 Å at 30 °C [68].
3. POPC: 1-palmitoyl-2-oleyl-*sn-glycero*-3-phosphatidylcholine, zwitterionic, A_{cross} = 68.3 Å^2 and D_{HH} = 37.0 Å at 30 °C [67].
4. POPE: 1-palmitoyl-2-oleoyl-*sn-glycero*-3- phosphoethanolamine, zwitterionic, A_{cross} = 56.0 Å^2 and D_{HH} = 41.3 Å at 30 °C [69].
5. POPS: 1-palmitoyl-2-oleoyl-*sn-glycero*-3-phosphoserine, anionic, A_{cross} = 55.0 Å^2 at 27 °C [70].
6. POPG: 1-palmitoyl-2-oleyl-*sn-glycero*-3-phosphatidylglycerol, anionic, A_{cross} = 62.8 Å^2 and D_{HH} = 36.0 Å at 37 °C [71].

The zwitterionic lipid bilayer is constituted with DOPC lipids. Various mixed lipid bilayers with combination of each zwitterionic and anionic lipid molecule, DOPS:POPE (1:2 mole ratio), POPC: POPS (3:1 mole ratio), and POPC:POPG (4:1 mole ratio) are used for representing the anionic bilayer system. For the mixed lipid bilayers, averaged values of A_{cross} and D_{HH} are taken based on a mole ratio.

3 Methods

Atomistic MD simulations with explicit atom representations for protein, lipid, water, and ion are performed using the CHARMM [72] program with the NAMD [73] parallelcomputing code on a Biowulf cluster at the National Institute of Health, Bethesda, MD (http://biowulf.nih.gov). Updated CHARMM [72] all-atom additive force field for lipids (C36) [74] and the modified TIP3P water model [75] are used to construct the set of starting points and to relax the systems to a production-ready stage. The bilayer system containing an Aβ channel/barrel, lipids, salts, and water normally has 200,000 atoms depending on the size of Aβ channel/ barrel. In the pre-equilibrium stages, a series of minimizations is performed for the initial configurations to remove overlaps of the alkane chains in the lipids and to gradually relax the solvents around the harmonically restrained peptides. The initial configurations are gradually relaxed through dynamic cycles with electrostatic cutoffs (12 Å). The harmonic restraints are gradually diminished with the full Ewald electrostatics calculation and constant temperature (Nosé—Hoover) thermostat/barostat at 303 K. For $t <$ 30 ns, our simulation employ the NPAT (constant number of atoms, pressure, surface area, and temperature) ensemble with a constant normal pressure applied in the direction perpendicular to the membrane. After $t = 30$ ns, the simulations employ the NPT ensemble. Production runs are generally performed up to 100 ns, and averages are taken after 30 ns, discarding initial transients.

3.1 Constructing Amvloid Channels

The initial channel models are constructed by using the U-shaped *β-strand-turn-β-strand* motifs and β-hairpins. The U-shaped peptide or the β-hairpin is subject to a multifold rotational symmetry operation with respect to the pore axis, creating the annular channel conformation. Depending on the direction of the rotation, the U-shaped peptide generates two different channel topologies: CNpNC (where C and N represent C- and N-terminal β-strands respectively, and p denotes a central pore) and NCpCN channels (Fig. 2a). In Aβ channels, the CNpNC channel preserves a central pore, while the NCpCN channel collapses the pore due to the hydrophobic mismatch of the charged N-terminal strands with the lipid bilayer hydrophobic core [30, 31] (*see* Note 1). However, in contrast to Aβ channels, K3 channels preserve the pore with NCpCN topology, while CNpNC K3 channel collapses the solvated pore due to the hydrophobic mismatch [43] (Fig. 2b). The U-shaped peptides yield a double-layered annular β-sheet [32, 35]. The designed channels have a perfectly annular shape with the pore-lining inner strands forming a β-sheet through intermolecular backbone hydrogen bonds (H-bonds), but the outer strands do not form a β-sheet due to the larger curvature at the channel periphery. In contrast, β-hairpins generate a single layered annular β-sheet [44, 45, 59] (Fig. 2c, d). Backbone H-bond formation is monitored during the simulations (*see* Note 2).

[1]In the simulations, pore structures can be examined by HOLE program [86]. The program allows us to visualize and analyze the pore or cavity in biomolecules such as ion channels.

[2]The time-dependent fraction of intermolecular (or intramolecular) backbone H-bonds, $Q_{H\text{-}bond}(t)$,for the β-sheet channels in the lipid bilayer can be calculated by

3.2 Generating Full-Length $A\beta_{1–42}$ Peptides

The NMR-derived U-shaped Aβ peptides only provide N-terminally truncated coordinates due to conformational disorder [50, 51]. To create full-length Aβ peptides, the $A\beta_{1–16}$ coordinates in the absence of Zn^{2+} (pdb code: 1ZE7) [76] are used for the missing N-terminal portions of the peptides. For each combination of the N-terminal structure with the NMR U-shaped motifs of $A\beta_{17–42}$ and $A\beta_{9–40}$, two $A\beta_{1–42}$ conformers were generated (Fig. 3). Conformer 1 has a turn at Ser26-Ile31, and conformer 2 at Asp23-Gly29. In the latter conformer, two C-terminal residues, Ile41 and Ala42, were added to create $A\beta_{1–42}$. Both $A\beta_{1–42}$ conformers retained the U-shaped β-strand-turn-β-strand motif and can be divided into four domains: the extramembranous N-terminal fragment (residues 1–16 and 1–8 for conformer 1 and 2, respectively), solvated pore-lining β-strand (residues 17–25 and 9–22 for conformer 1 and 2, respectively), turn (residues 26–31 and 23–29 for conformer 1 and 2, respectively), and lipid-interacting C-terminal β-strand (residues 32–42 and 30–42 for conformer 1 and 2, respectively).

3.3 β-Barrel Topology of Aβ Channels

Amyloid channels can have conventional annular β-sheet channel and β-barrel topologies. To construct the channel structure with the conventional β-strands arrangement, monomers (U-shaped peptides or β-hairpins) were inserted without inclination with respect to the membrane normal, generating the annular channel topology (Figs. 2 and 4a). To construct the β-barrel structure, the monomers were inclined ~37° with respect to the pore axis, creating the β-barrel topology [34] (Fig. 4b). The β-barrel morphology mimics naturally occurring β-barrels observed in transmembrane proteins that are found frequently in the outer membranes of bacteria, mitochondria, and chloroplasts. The β-barrel motif is a large β-sheet composed of an even number of β-strands. Some known structures of β-barrel membrane proteins have β-strands ranging in number from 8 to 22 [77, 78] (*see* Note 3). Examples are shown here for the U-shaped amyloid β-barrels and β-hairpin barrels (Fig. 4c). In the simulations, the initial annular conformation is gradually lost during the relaxation of the lipid bilayer. No peptide dissociation from the barrels is observed at these time scales. The relaxed barrel conformation with localized β-sheet optimization leads to subunit formations. Heterogeneity in barrel conformations can be evaluated by several criteria (*see* Note 4).

$$Q_{\text{H–bond}}(t) = \frac{N_{\text{H–bond}}}{N_{\text{H–bond}}^{\max}}$$

where $N_{\text{H-bond}}$ is the number of intermolecular H-bonds at each time frame, and $N_{\text{H–bond}}^{\max}$ is the maximum possible number of the backbone H-bonds as monitored in the initial configuration.

[3]Aβ channels/barrels were modeled with 12–36 Aβ peptides. Different numbers of Aβ monomers produced channels/barrels with different outer and pore dimensions. Preferred sizes of Aβ channels/barrels were found to be in the range of 16–24 Aβ peptides, i.e., 16–24 β-strands lining the pores. The smaller one (12-mer) collapsed and the larger one (36-mer) was not supported by the bilayer [32, 35]. This range was also found to hold for other toxic β-sheet channels; K3 channels with 24 β-strands [43], 18- and 24-mer human islet amyloid polypeptide (hIAPP) channels [87], PG-1 channels with 16–20 β-strands [44, 45], and MAX channels with 20 β-strands [59].

3.4 D-Enantiomer $A\beta_{1–42}$ Peptides

The standard CHARMM force field [72] is primarily designed for L-amino acids ("left-handed" isomers). To simulate D-amino acids ("right-handed" isomers), a protein force field for asymmetric isomers is required. D-amino acid is a mirror image of L-amino acid, indicating that they are identical, except for their backbone chirality. In the simulations, the L- and D-amino acids share the same backbone bonds and angles, indicating that the standard L-amino acids parameters can be used for the D-amino acids. However, the parameters include the dihedral angle cross term map (CMAP) correction [79], which was created for only L-amino acids, and cannot be directly applied to D-amino acids. Thus, in the simulation, a mirror-image CMAP term for D-amino acids reflecting the phi-psi CMAP matrix should be used [80]. Current version of CHARMM36 force field supports D-amino acids simulations.

3.5 Aβ Mutants

Naturally occurring point mutations in the amyloid precursor protein (APP) clustered around the central region of the Aβ residues are related to familial forms of AD [81]. However, designed synthetic point substitutions significantly alter the channel activity, suppressing Aβ toxicity.

1. F19P and F20C point substitutions: Two phenylalanine residues, Phe19 and Phe20, were replaced with Pro19 and Cys20, respectively (Fig. 5a). The F19P substitution in both truncated $A\beta_{17–42}$ and full-length $A\beta_{1–42}$ channels/barrels prevents pore activity and hence cellular toxicity, while the F20C substitution preserves the solvated pore with channel activity comparable to the wild type [33, 37, 39].
2. Unlike point substitution, Osaka mutant (ΔE22) eliminates residue Glu22 from the pore-lining β-strand [40]. As a result, pore-lining residues 10–21 for both conformers flip their side chains, while the other domains remain intact (Fig. 5b). The ΔE22 barrels show the membrane embedded β-sheet channel topology, indistinguishable from the wild-type $A\beta_{1–42}$ barrels.

3.6 Pyroglutamate (pE) Modified Aβ Peptides

Pyroglutamate-modified Aβ ($A\beta_{pE3–42}$) peptide is particularly associated with cytotoxicity in AD [82, 83]. The peptide is posttranslationally generated by cleavage of the first two N-terminal amino acids (Asp1 and Ala2) of $A\beta_{1–42}$, leaving an exposed Glu3 residue. Intramolecular dehydration catalyzed by the glutaminyl cyclase (QC) enzyme generates a lactam ring in Glu3, converting to the pyroglutamate (pE) residue [82, 83]. To simulate

[4]The β-sheet secondary structure was determined by the STRIDE program [88]. "Straightness" of the strand was calculated by β-strand order parameter, $S_\beta = \frac{1}{N_V}\sum_{k=1}^{N_V}\left(\frac{3\cos^2\theta_\alpha - 1}{2}\right)$ where θ_α is the angle between the positional vectors connecting two C_α atoms, and N_V is the total number of vector pairs. The averaged β-strand *B*-factor (or Temperature factor) was calculated from the root-mean-squared (RMS) fluctuations [89] relative to the starting point during the simulations with a simple correlation of $B = 8\pi^2\frac{\langle \mathrm{RMSF}\rangle^2}{3}$ where $\langle\ \rangle$ denotes averaging over simulation time. Percent of β-sheet content based on the intermolecular backbone H-bonds between β-strands was calculated.

pyroglutamate (pE), the first two residues, Asp1 and Ala2, from each conformer 1 and 2 of $A\beta_{1-42}$ peptide are removed. The Glu3 residue is then converted into pE3 by generating the lactam ring (Fig. 6). The pE molecular topology was generated by the Avogadro software [84], since the pE residue is not included in the standard CHARMM [72] force field protocol. The Gaussian09 program [85] can be used to calculate parameters including partial charges, bond lengths, angles, and torsional angles for the atoms in the pE residue. The calculated parameters can be directly adopted in the CHARMM [72] program.

3.7 Calculating Aβ Pore Activity

Amyloid channels/barrels preserve a large pore, ~1–2 nm, wide enough for conducting ions and water. In addition to counter ions to the system for neutralization, the bilayer systems contain Mg^{2+}, K^+, Ca^{2+}, and Zn^{2+} at the same concentration of 25 mM to satisfy a total cation concentration near 100 mM, as well as Cl^-, which mimics the physiological salt concentration. Cations can be trapped by the negatively charged amino acids in the solvated pore. The motions of the cations in the pore, which reflect the electrostatic interaction, can delineate the electrophysiological currents across the membrane. Several quantities calculated from the simulations can provide detailed information of the mechanism for ion permeation across the bilayer.

1. Probability distribution functions, P, for ions representing ionic permeation as a function of the distance along the pore center axis can be calculated over the simulations. Peaks in the distribution curve represent the cationic binding sites [30, 34, 40, 45, 59].
2. In order to see the ions' behavior in the pore, the potential of mean force (PMF), ΔG_{PMF}, representing the relative free energy profile for each ion across the bilayer can be calculated [32–35, 44] (*see* Note 5).
3. To observe ion fluctuation across the pore, the change in total charge, $\Delta Q\,(C/\mathrm{ns})$, in the pore as a function of the simulation time can be calculated. In the calculations, different pore lengths with different cutoffs along the pore axis are used [36, 37, 40, 42].
4. To correlate the charge fluctuations with experimental ion conductance, the maximum conductance, $g_{\max}$, representing the ion transport can be calculated from the equilibrium simulations [36, 42] (*see* Note 6).

---

[5]The PMF is calculated by using the equation of $\Delta G_{\mathrm{PMF}}(\overrightarrow{r}) = -k_{\mathrm{B}}T\ln\left(\rho(\overrightarrow{r})/\rho_{\mathrm{bulk}}\right)$. Here, k_{B} is the Boltzmann constant, T is the simulation temperature, $\rho(\overrightarrow{r})$ is the equilibrium number density of ions, and ρ_{bulk} is the averaged ion density in the bulk region. Accurate equilibrium PMF relevant to ion permeation should be obtained from free energy calculations with the umbrella sampling method [90]. Nevertheless, given the simulation trajectory without additional multiple equilibrium runs for sampling, ion-density-based PMF calculations are useful to obtain an estimate of the relative free energy changes for ions, providing an outline for pore ion permeation [91, 92].

[6]For the equilibrium all-atom MD simulations in the absence of membrane potentials, the maximum conductance, $g_{\max}$, [93] representing the ion transport can be described as

$$g_{\max} = \frac{q_e^2}{k_{\mathrm{B}}TL^2}\langle D(z)e^{G_{\mathrm{PMF}}(z)/k_{\mathrm{B}}T}\rangle^{-1}\langle e^{-G_{\mathrm{PMF}}(z)/k_{\mathrm{B}}T}\rangle^{-1}$$

Acknowledgements

This project has been funded in whole or in part with Federal funds from the Frederick National Laboratory for Cancer Research, National Institutes of Health, under contract HHSN261200800001E. This research was supported [in part] by the Intramural Research Program of NIH, Frederick National Lab, Center for Cancer Research. The content of this publication does not necessarily reflect the views or policies of the Department of Health and Human Services, nor does mention of trade names, commercial products or organizations imply endorsement by the US Government.

References

1. Monsonego A, Zota V, Karni A, Krieger JI, Bar-Or A, Bitan G, Budson AE, Sperling R, Selkoe DJ, Weiner HL (2003) Increased T cell reactivity to amyloid beta protein in older humans and patients with Alzheimer disease. J Clin Invest 112:415–422 [PubMed: 12897209]
2. Cohen FE, Kelly JW (2003) Therapeutic approaches to protein-misfolding diseases. Nature 426:905–909 [PubMed: 14685252]
3. Temussi PA, Masino L, Pastore A (2003) From Alzheimer to Huntington: why is a structural understanding so difficult? EMBO J 22:355–361 [PubMed: 12554637]
4. Dobson CM (2003) Protein folding and misfolding. Nature 426:884–890 [PubMed: 14685248]
5. Chiti F, Dobson CM (2006) Protein misfolding, functional amyloid, and human disease. Annu Rev Biochem 75:333–366 [PubMed: 16756495]
6. DeToma AS, Salamekh S, Ramamoorthy A, Lim MH (2012) Misfolded proteins in Alzheimer's disease and type II diabetes. Chem Soc Rev 41:608–621 [PubMed: 21818468]
7. Eisenberg D, Jucker M (2012) The amyloid state of proteins in human diseases. Cell 148: 1188–1203 [PubMed: 22424229]
8. Jang H, Arce FT, Ramachandran S, Kagan BL, Lal R, Nussinov R (2014) Disordered amyloidogenic peptides may insert into the membrane and assemble into common cyclic structural motifs. Chem Soc Rev 43:6750–6764 [PubMed: 24566672]
9. Marshall KE, Serpell LC (2010) Fibres, crystals and polymorphism: the structural promiscuity of amyloidogenic peptides. Soft Matter 6:2110–2114
10. Miller Y, Ma B, Nussinov R (2010) Polymorphism in Alzheimer Abeta amyloid organization reflects conformational selection in a rugged energy landscape. Chem Rev 110: 4820–4838 [PubMed: 20402519]
11. Sipe JD, Cohen AS (2000) Review: history of the amyloid fibril. J Struct Biol 130:88–98 [PubMed: 10940217]
12. Quist A, Doudevski I, Lin H, Azimova R, Ng D, Frangione B, Kagan B, Ghiso J, Lal R (2005) Amyloid ion channels: a common structural link for protein-misfolding disease. Proc Natl Acad Sci U S A 102:10427–10432 [PubMed: 16020533]
13. Glabe CG (2008) Structural classification of toxic amyloid oligomers. J Biol Chem 283: 29639–29643 [PubMed: 18723507]
14. Bernstein SL, Dupuis NF, Lazo ND, Wyttenbach T, Condron MM, Bitan G, Teplow DB, Shea JE, Ruotolo BT, Robinson CV, Bowers MT (2009) Amyloid-beta protein oligomerization and the importance of tetramers and dodecamers in the aetiology of Alzheimer's disease. Nat Chem 1:326–331 [PubMed: 20703363]
15. Butterfield SM, Lashuel HA (2010) Amyloidogenic protein-membrane interactions: mechanistic insight from model systems. Angew Chem Int Ed Engl 49:5628–5654 [PubMed: 20623810]
16. Matsumura S, Shinoda K, Yamada M, Yokojima S, Inoue M, Ohnishi T, Shimada T, Kikuchi K, Masui D, Hashimoto S, Sato M, Ito A, Akioka M, Takagi S, Nakamura Y, Nemoto K, Hasegawa Y, Takamoto H, Inoue H, Nakamura S, Nabeshima Y, Teplow DB, Kinjo M, Hoshi M (2011) Two distinct amyloid beta-protein (Abeta) assembly pathways leading to oligomers and fibrils

where q_e^2 is the elementary charge, k_B denotes the Boltzmann's constant, T is the simulation temperature, and L represents the pore length. In the bracket, $D(z)$ and $\Delta G_{PMF}(z)$ denote the one-dimensional diffusion coefficient and the one-dimensional potential of mean force for ions, respectively. The bracket averages over the pore length L.

identified by combined fluorescence correlation spectroscopy, morphology, and toxicity analyses. J Biol Chem 286:11555–11562 [PubMed: 21292768]

17. Relini A, Cavalleri O, Rolandi R, Gliozzi A (2009) The two-fold aspect of the interplay of amyloidogenic proteins with lipid membranes. Chem Phys Lipids 158:1–9 [PubMed: 19056366]
18. Garner B (2010) Lipids and Alzheimer's disease. Biochim Biophys Acta 1801:747–749 [PubMed: 20547302]
19. Williams TL, Serpell LC (2011) Membrane and surface interactions of Alzheimer's A beta peptide—insights into the mechanism of cytotoxicity. FEBS J 278:3905–3917 [PubMed: 21722314]
20. Verdier Y, Zarandi M, Penke B (2004) Amyloid beta-peptide interactions with neuronal and glial cell plasma membrane: binding sites and implications for Alzheimer's disease. J Pept Sci 10:229–248 [PubMed: 15160835]
21. Shirwany NA, Payette D, Xie J, Guo Q (2007) The amyloid beta ion channel hypothesis of Alzheimer's disease. Neuropsychiatr Dis Treat 3:597–612 [PubMed: 19300589]
22. Buchete NV (2012) Unlocking the atomic-level details of amyloid fibril growth through advanced biomolecular simulations. Biophys J 103:1411–1413 [PubMed: 23062332]
23. Walsh DM, Klyubin I, Fadeeva JV, Cullen WK, Anwyl R, Wolfe MS, Rowan MJ, Selkoe DJ (2002) Naturally secreted oligomers of amyloid beta protein potently inhibit hippocampal long-term potentiation in vivo. Nature 416:535–539 [PubMed: 11932745]
24. Kagan BL (2012) Membrane pores in the pathogenesis of neurodegenerative disease. Prog Mol Biol Transl Sci 107:295–325 [PubMed: 22482454]
25. Arispe N, Pollard HB, Rojas E (1993) Giant multilevel cation channels formed by Alzheimer disease amyloid beta-protein [A beta P-(1–40)] in bilayer membranes. Proc Natl Acad Sci U S A 90:10573–10577 [PubMed: 7504270]
26. Arispe N, Rojas E, Pollard HB (1993) Alzheimer disease amyloid β protein forms calcium channels in bilayer membranes: blockade by tromethamine and aluminum. Proc Natl Acad Sci U S A 90:567–571 [PubMed: 8380642]
27. Arispe N, Pollard HB, Rojas E (1994) The ability of amyloid beta-protein [a-Beta-P(1–40)] to form Ca^{2+} channels provides a mechanism for neuronal death in Alzheimer's disease. Ann N Y Acad Sci 747:256–266 [PubMed: 7847675]
28. Arispe N, Pollard HB, Rojas E (1996) Zn^{2+} interaction with Alzheimer amyloid β protein calcium channels. Proc Natl Acad Sci U S A 93:1710–1715 [PubMed: 8643694]
29. Lin H, Bhatia R, Lal R (2001) Amyloid β protein forms ion channels: implications for Alzheimer's disease pathophysiology. FASEB J 15:2433–2444 [PubMed: 11689468]
30. Jang H, Zheng J, Nussinov R (2007) Models of β-amyloid ion channels in the membrane suggest that channel formation in the bilayer is a dynamic process. Biophys J 93:1938–1949 [PubMed: 17526580]
31. Jang H, Zheng J, Lal R, Nussinov R (2008) New structures help the modeling of toxic amyloidβ ion channels. Trends Biochem Sci 33:91–100 [PubMed: 18182298]
32. Jang H, Arce FT, Capone R, Ramachandran S, Lal R, Nussinov R (2009) Misfolded amyloid ion channels present mobile β-sheet subunits in contrast to conventional ion channels. Biophys J 97:3029–3037 [PubMed: 19948133]
33. Jang H, Arce FT, Ramachandran S, Capone R, Azimova R, Kagan BL, Nussinov R, Lal R (2010) Truncated β-amyloid peptide channels provide an alternative mechanism for Alzheimer's disease and down syndrome. Proc Natl Acad Sci U S A 107:6538–6543 [PubMed: 20308552]
34. Jang H, Arce FT, Ramachandran S, Capone R, Lal R, Nussinov R (2010) β-Barrel topology of Alzheimer's β-amyloid ion channels. J Mol Biol 404:917–934 [PubMed: 20970427]
35. Jang H, Teran Arce F, Ramachandran S, Capone R, Lal R, Nussinov R (2010) Structural convergence among diverse, toxic β-sheet ion channels. J Phys Chem B 114:9445–9451 [PubMed: 20608696]
36. Capone R, Jang H, Kotler SA, Connelly L, Teran Arce F, Ramachandran S, Kagan BL, Nussinov R, Lal R (2012) All-D-enantiomer of β-amyloid peptide forms ion channels in lipid bilayers. J Chem Theory Comput 8:1143–1152 [PubMed: 22423218]

37. Capone R, Jang H, Kotler SA, Kagan BL, Nussinov R, Lal R (2012) Probing structural features of Alzheimer's amyloid-β pores in bilayers using site-specific amino acid substitutions. Biochemistry 51:776–785 [PubMed: 22242635]
38. Connelly L, Jang H, Arce FT, Capone R, Kotler SA, Ramachandran S, Kagan BL, Nussinov R, Lal R (2012) Atomic force microscopy and MD simulations reveal pore-like structures of all-D-enantiomer of Alzheimer's β-amyloid peptide: relevance to the ion channel mechanism of AD pathology. J Phys Chem B 116:1728–1735 [PubMed: 22217000]
39. Connelly L, Jang H, Arce FT, Ramachandran S, Kagan BL, Nussinov R, Lal R (2012) Effects of point substitutions on the structure of toxic Alzheimer's β-amyloid channels: atomic force microscopy and molecular dynamics simulations. Biochemistry 51:3031–3038 [PubMed: 22413858]
40. Jang H, Arce FT, Ramachandran S, Kagan BL, Lal R, Nussinov R (2013) Familial Alzheimer's disease Osaka mutant (ΔE22) β-barrels suggest an explanation for the different Aβ1–40/42 preferred conformational states observed by experiment. J Phys Chem B 117:11518–11529 [PubMed: 24000923]
41. Jang H, Connelly L, Arce FT, Ramachandran S, Lal R, Kagan BL, Nussinov R (2013) Alzheimer's disease: which type of amyloid-preventing drug agents to employ? Phys Chem Chem Phys 15:8868–8877 [PubMed: 23450150]
42. Gillman AL, Jang H, Lee J, Ramachandran S, Kagan BL, Nussinov R, Teran Arce F (2014) Activity and architecture of pyroglutamate-modified amyloid-β (AβpE3–42) pores. J Phys Chem B 118:7335–7344 [PubMed: 24922585]
43. Mustata M, Capone R, Jang H, Arce FT, Ramachandran S, Lal R, Nussinov R (2009) K3 fragment of amyloidogenic β2-microglobulin forms ion channels: implication for dialysis related amyloidosis. J Am Chem Soc 131: 14938–14945 [PubMed: 19824733]
44. Jang H, Ma B, Lal R, Nussinov R (2008) Models of toxic β-sheet channels of protegrin-1 suggest a common subunit organization motif shared with toxic Alzheimer β-amyloid ion channels. Biophys J 95:4631–4642 [PubMed: 18708452]
45. Capone R, Mustata M, Jang H, Arce FT, Nussinov R, Lal R (2010) Antimicrobial protegrin-1 forms ion channels: molecular dynamic simulation, atomic force microscopy, and electrical conductance studies. Biophys J 98:2644–2652 [PubMed: 20513409]
46. Jang H, Connelly L, Arce FT, Ramachandran S, Kagan BL, Lal R, Nussinov R (2013) Mechanisms for the insertion of toxic, fibril-like β-amyloid oligomers into the membrane. J Chem Theory Comput 9:822–833 [PubMed: 23316126]
47. Ladiwala AR, Litt J, Kane RS, Aucoin DS, Smith SO, Ranjan S, Davis J, Vannostrand WE, Tessier PM (2012) Conformational differences between two amyloid beta oligomers of similar size and dissimilar toxicity. J Biol Chem 287: 24765–24773 [PubMed: 22547072]
48. Chimon S, Shaibat MA, Jones CR, Calero DC, Aizezi B, Ishii Y (2007) Evidence of fibril-like beta-sheet structures in a neurotoxic amyloid intermediate of Alzheimer's beta-amyloid. Nat Struct Mol Biol 14:1157–1164 [PubMed: 18059284]
49. Ma B, Nussinov R (2002) Stabilities and conformations of Alzheimer's β-amyloid peptide oligomers (Aβ16–22, Aβ16–35, and Aβ10–35): sequence effects. Proc Natl Acad Sci U S A 99:14126–14131 [PubMed: 12391326]
50. Lührs T, Ritter C, Adrian M, Riek-Loher D, Bohrmann B, Doeli H, Schubert D, Riek R (2005) 3D structure of Alzheimer's amyloid-β(1–42) fibrils. Proc Natl Acad Sci U S A 102: 17342–17347 [PubMed: 16293696]
51. Petkova AT, Yau WM, Tycko R (2006) Experimental constraints on quaternary structure in Alzheimer's β-amyloid fibrils. Biochemistry 45:498–512 [PubMed: 16401079]
52. Bertini I, Gonnelli L, Luchinat C, Mao J, Nesi A (2011) A new structural model of Aβ40 fibrils. J Am Chem Soc 133:16013–16022 [PubMed: 21882806]
53. Iwata K, Fujiwara T, Matsuki Y, Akutsu H, Takahashi S, Naiki H, Goto Y (2006) 3D structure of amyloid protofilaments of β2-microglobulin fragment probed by solid-tate NMR. Proc Natl Acad Sci U S A 103: 18119–18124 [PubMed: 17108084]
54. Zheng J, Jang H, Ma B, Nussinov R (2008) Annular structures as intermediates in fibril formation of Alzheimer Aβ17–42. J Phys Chem B 112:6856–6865 [PubMed: 18457440]

55. Zheng J, Jang H, Nussinov R (2008) β2-microglobulin amyloid fragment organization and morphology and its comparison to Aβ suggests that amyloid aggregation pathways are sequence specific. Biochemistry 47:2497–2509 [PubMed: 18215070]
56. Arce FT, Jang H, Ramachandran S, Landon PB, Nussinov R, Lal R (2011) Polymorphism of amyloid β peptide in different environments: implications for membrane insertion and pore formation. Soft Matter 7:5267–5273 [PubMed: 21918653]
57. Lee J, Gillman AL, Jang H, Ramachandran S, Kagan BL, Nussinov R, Teran Arce F (2014) Role of the fast kinetics of pyroglutamate-modified amyloid-β oligomers in membrane binding and membrane permeability. Biochemistry 53:4704–4714 [PubMed: 24950761]
58. Ferguson N, Becker J, Tidow H, Tremmel S, Sharpe TD, Krause G, Flinders J, Petrovich M, Berriman J, Oschkinat H, Fersht AR (2006) General structural motifs of amyloid protofilaments. Proc Natl Acad Sci U S A 103: 16248–16253 [PubMed: 17060612]
59. Gupta K, Jang H, Harlen K, Puri A, Nussinov R, Schneider JP, Blumenthal R (2013) Mechanism of membrane permeation induced by synthetic β-hairpin peptides. Biophys J 105: 2093–2103 [PubMed: 24209854]
60. Miyasaki KT, Lehrer RI (1998) Beta-sheet antibiotic peptides as potential dental therapeutics. Int J Antimicrob Agents 9:269–280 [PubMed: 9573496]
61. Roumestand C, Louis V, Aumelas A, Grassy G, Calas B, Chavanieu A (1998) Oligomerization of protegrin-1 in the presence of DPC micelles. A proton high-resolution NMR study. FEBS Lett 421:263–267 [PubMed: 9468319]
62. Fahrner RL, Dieckmann T, Harwig SS, Lehrer RI, Eisenberg D, Feigon J (1996) Solution structure of protegrin-1, a broad-spectrum antimicrobial peptide from porcine leukocytes. Chem Biol 3:543–550 [PubMed: 8807886]
63. Jang H, Ma B, Woolf TB, Nussinov R (2006) Interaction of protegrin-1 with lipid bilayers: membrane thinning effect. Biophys J 91: 2848–2859 [PubMed: 16861271]
64. Jang H, Ma B, Nussinov R (2007) Conformational study of the protegrin-1 (PG-1) dimer interaction with lipid bilayers and its effect. BMC Struct Biol 7:21 [PubMed: 17407565]
65. Woolf TB, Roux B (1994) Molecular dynamics simulation of the gramicidin channel in a phospholipid bilayer. Proc Natl Acad Sci U S A 91:11631–11635 [PubMed: 7526400]
66. Woolf TB, Roux B (1996) Structure, energetics, and dynamics of lipid-protein interactions: a molecular dynamics study of the gramicidin A channel in a DMPC bilayer. Proteins 24: 92–114 [PubMed: 8628736]
67. Kucerka N, Tristram-Nagle S, Nagle JF (2005) Structure of fully hydrated fluid phase lipid bilayers with monounsaturated chains. J Membr Biol 208:193–202 [PubMed: 16604469]
68. Petrache HI, Tristram-Nagle S, Gawrisch K, Harries D, Parsegian VA, Nagle JF (2004) Structure and fluctuations of charged phosphatidylserine bilayers in the absence of salt. Biophys J 86:1574–1586 [PubMed: 14990484]
69. Rand RP, Parsegian VA (1989) Hydration forces between phospholipid-bilayers. Biochim Biophys Acta 988:351–376
70. Mukhopadhyay P, Monticelli L, Tieleman DP (2004) Molecular dynamics simulation of a palmitoyl-oleoyl phosphatidylserine bilayer with Na^+ counterions and NaCl. Biophys J 86: 1601–1609 [PubMed: 14990486]
71. Rog T, Murzyn K, Pasenkiewicz-Gierula M (2003) Molecular dynamics simulations of charged and neutral lipid bilayers: treatment of electrostatic interactions. Acta Biochim Pol 50:789–798 [PubMed: 14515159]
72. Brooks BR, Bruccoleri RE, Olafson BD, States DJ, Swaminathan S, Karplus M (1983) CHARMM—a program for macromolecular energy, minimization, and dynamics calculations. J Comp Chem 4:187–217
73. Phillips JC, Braun R, Wang W, Gumbart J, Tajkhorshid E, Villa E, Chipot C, Skeel RD, Kale L, Schulten K (2005) Scalable molecular dynamics with NAMD. J Comp Chem 26: 1781–1802 [PubMed: 16222654]
74. Klauda JB, Venable RM, Freites JA, O'Connor JW, Tobias DJ, Mondragon-Ramirez C, Vorobyov I, MacKerell AD, Pastor RW (2010) Update of the CHARMM all-atom additive force field for lipids: validation on six lipid types. J Phys Chem B 114:7830–7843 [PubMed: 20496934]

75. Durell SR, Brooks BR, Bennaim A (1994) Solvent-induced forces between two hydrophilic groups. J Phys Chem 98:2198–2202
76. Zirah S, Kozin SA, Mazur AK, Blond A, Cheminant M, Segalas-Milazzo I, Debey P, Rebuffat S (2006) Structural changes of region 1–16 of the Alzheimer disease amyloid β-peptide upon zinc binding and in vitro aging. J Biol Chem 281:2151–2161 [PubMed: 16301322]
77. Schulz GE (2002) The structure of bacterial outer membrane proteins. Biochim Biophys Acta 1565:308–317 [PubMed: 12409203]
78. Sansom MS, Kerr ID (1995) Transbilayer pores formed by beta-barrels: molecular modeling of pore structures and properties. Biophys J 69:1334–1343 [PubMed: 8534803]
79. Mackerell AD, Feig M, Brooks CL (2004) Extending the treatment of backbone energetics in protein force fields: limitations of gas- phase quantum mechanics in reproducing protein conformational distributions in molecular dynamics simulations. J Comput Chem 25:1400–1415 [PubMed: 15185334]
80. Connelly L, Jang H, Teran Arce F, Capone R, Kotler SA, Ramachandran S, Kagan BL, Nussinov R, Lal R (2012) Atomic force microscopy and MD simulations reveal pore-like structures of all-D-enantiomer of Alzheimer's beta-amyloid peptide relevance to the ion channel mechanism of AD pathology. J Phys Chem B. doi:10.1021/jp2108126
81. de Groot NS, Aviles FX, Vendrell J, Ventura S (2006) Mutagenesis of the central hydrophobic cluster in Abeta42 Alzheimer's peptide. Side-chain properties correlate with aggregation propensities. FEBS J 273:658–668 [PubMed: 16420488]
82. Jawhar S, Wirths O, Bayer TA (2011) Pyroglutamate amyloid-β (Aβ): a hatchet man in Alzheimer disease. J Biol Chem 286: 38825–38832 [PubMed: 21965666]
83. Saido TC, Iwatsubo T, Mann DMA, Shimada H, Ihara Y, Kawashima S (1995) Dominant and differential deposition of distinct β-amyloid peptide species, a-beta(N3(Pe)), in senile plaques. Neuron 14:457–466 [PubMed: 7857653]
84. Hanwell MD, Curtis DE, Lonie DC, Vandermeersch T, Zurek E, Hutchison GR (2012) Avogadro: an advanced semantic chemical editor, visualization, and analysis platform. J Cheminform 4:17 [PubMed: 22889332]
85. Frisch MJ, Trucks GW, Schlegel HB, Scuseria GE, Robb MA, Cheeseman JR, Scalmani G, Barone V, Mennucci B, Petersson GA, Nakatsuji H, Caricato M, Li X, Hratchian HP, Izmaylov AF, Bloino J, Zheng G, Sonnenberg JL, Hada M, Ehara M, Toyota K, Fukuda R, Hasegawa J, Ishida M, Nakajima T, Honda Y, Kitao O, Nakai H, Vreven T, Montgomery JA, Peralta JE, Ogliaro F, Bearpark M, Heyd JJ, Brothers E, Kudin KN, Staroverov VN, Kobayashi R, Normand J, Raghavachari K, Rendell A, Burant JC, Iyengar SS, Tomasi J, Cossi M, Rega N, Millam JM, Klene M, Knox JE, Cross JB, Bakken V, Adamo C, Jaramillo J, Gomperts R, Stratmann RE, Yazyev O, Austin AJ, Cammi R, Pomelli C, Ochterski JW, Martin RL, Morokuma K, Zakrzewski VG, Voth GA, Salvador P, Dannenberg JJ, Dapprich S, Daniels AD, Farkas Ö, Foresman JB, Ortiz JV, Cioslowski J, Fox DJ (2009) Gaussian 09, Revision B.01 Wallingford CT
86. Smart OS, Goodfellow JM, Wallace BA (1993) The pore dimensions of gramicidin-A. Biophys J 65:2455–2460 [PubMed: 7508762]
87. Zhao J, Luo Y, Jang H, Yu X, Wei G, Nussinov R, Zheng J (2012) Probing ion channel activity of human islet amyloid polypeptide (amylin). Biochim Biophys Acta 1818:3121–3130 [PubMed: 22935354]
88. Frishman D, Argos P (1995) Knowledge-based protein secondary structure assignment. Proteins 23:566–579 [PubMed: 8749853]
89. Wriggers W, Mehler E, Pitici F, Weinstein H, Schulten K (1998) Structure and dynamics of calmodulin in solution. Biophys J 74: 1622–1639 [PubMed: 9545028]
90. Allen TW, Andersen OS, Roux B (2006) Molecular dynamics—potential of mean force calculations as a tool for understanding ion permeation and selectivity in narrow channels. Biophys Chem 124:251–267 [PubMed: 16781050]
91. de Groot BL, Grubmuller H (2001) Water permeation across biological membranes: mechanism and dynamics of aquaporin-1 and GlpF. Science 294:2353–2357 [PubMed: 11743202]
92. Leontiadou H, Mark AE, Marrink SJ (2007) Ion transport across transmembrane pores. Biophys J 92:4209–4215 [PubMed: 17384063]

93. Allen TW, Andersen OS, Roux B (2004) Energetics of ion conduction through the gramicidin channel. Proc Natl Acad Sci U S A 101:117–122 [PubMed: 14691245]

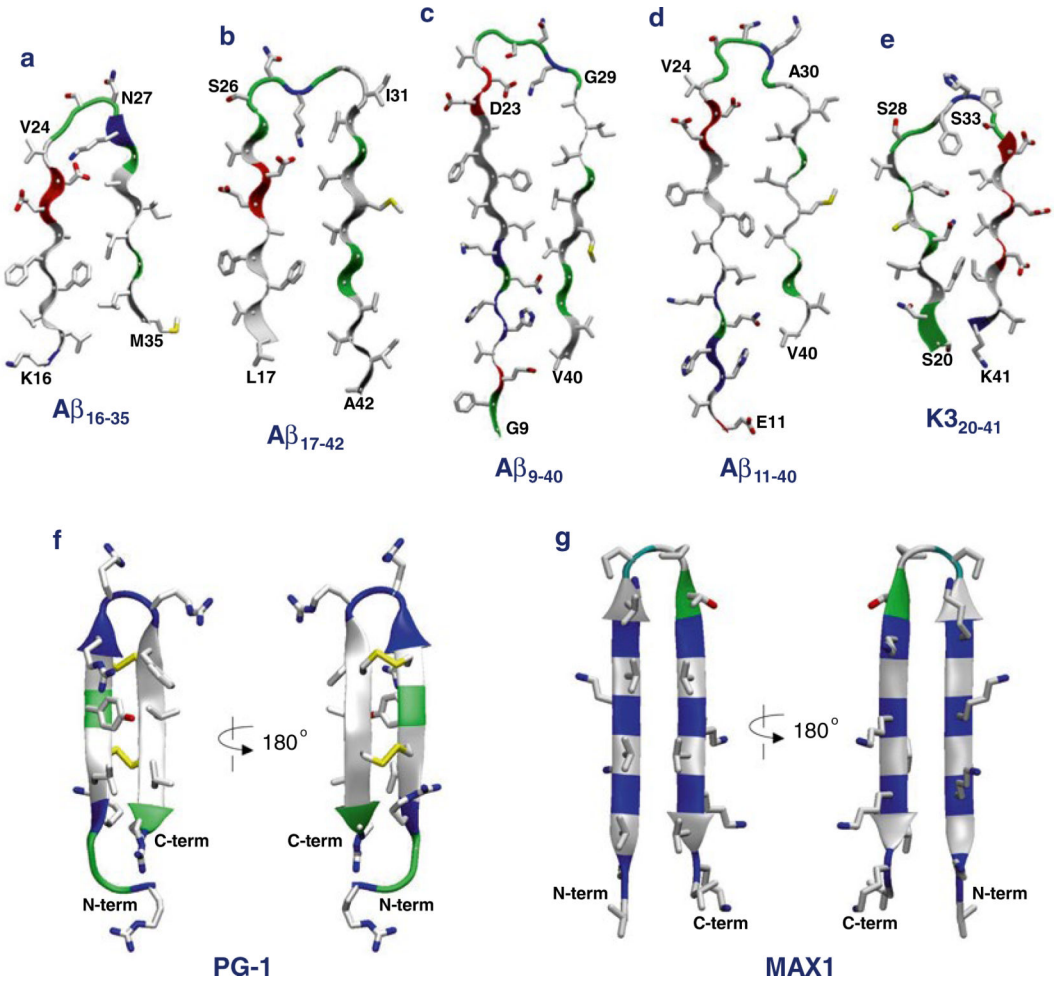

Fig. 1.

Monomer conformations recruited for the molecular dynamics (MD) simulations of β-sheet channels in the lipid bilayers. The U-shaped amyloid peptides with the *β-strand-turn-β-strand* motif for (**a**) the computational $A\beta_{16–35}$, (**b**) the NMR-derived $A\beta_{17–42}$, (**c**) the ssNMR $A\beta_{9–40}$, (**d**) the ssNMR $A\beta_{11–40}$, and (**e**) the ssNMR $K3_{20–41}$ peptides. The β-hairpin motif for the synthetic (**f**) protegrin-1 (PG-1) and (**g**) MAX1 peptides. In the peptide ribbon, hydrophobic, polar/Gly, positively charged, and negatively charged residues are colored *white, green, blue*, and *red*, respectively. *Yellow sticks* in PG-1 denote the disulfide bonds

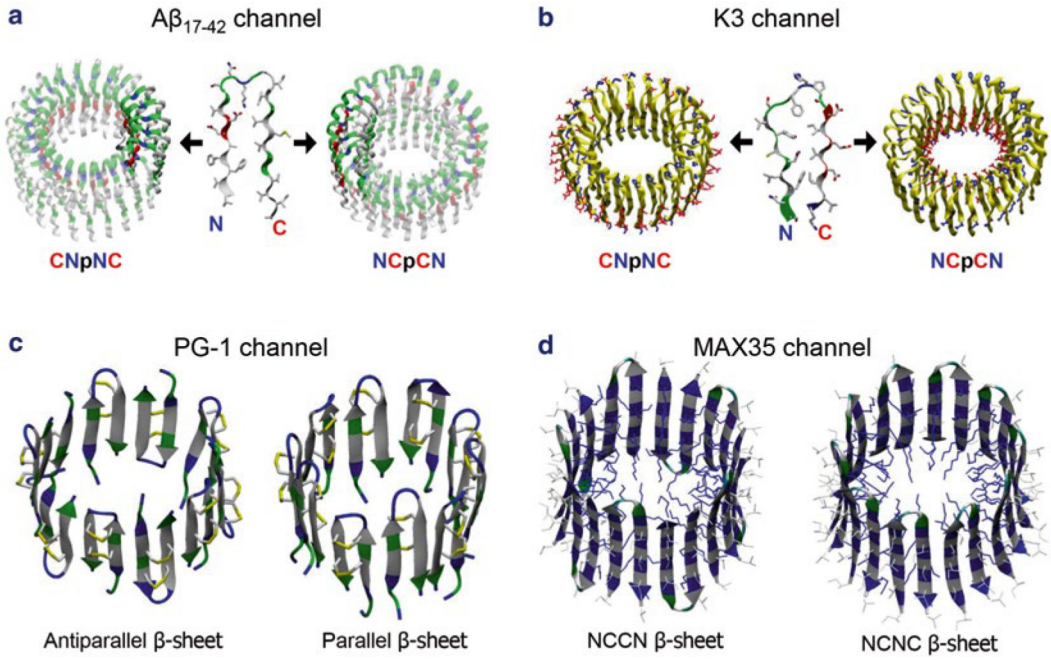

Fig. 2.

Computational models of β-sheet channel with the U-shaped and β-hairpin motifs. (**a**) Building annular channel structures in the membrane using (**a**) the NMR-based $A\beta_{17–42}$ and(**b**) the ssNMR $K3_{20–41}$ peptides. In the double-layered β-sheet channels, two different directions of peptide addition along the curvature yield the CNpNC (*left*) and NCpCN (*right*) channels (here, C: C-terminal, N: N-terminal, p: pore). Unlike the U-shaped peptides, β-hairpins generate a single layered annular β-sheet for (**c**) protegrin-1 (PG-1) and (**d**) MAX 35 channels. The PG-1 channels contain the antiparallel (turn-next-to-tail, *left*) and parallel (turn-next-to-turn, *right*) β-sheet arrangements in an NCCN packing mode. In the MAX channels, the β-hairpin arrangements give rise to two potential β-sheet motifs; turn-next-to-tail β-hairpins in NCCN packing mode (*left*) and turn-next-to-turn β-hairpins in NCNC packing mode (*right*). In both cases, the MAX β-hairpins form antiparallel β-sheets, positioning the positively charged Lys side chains into the central pore

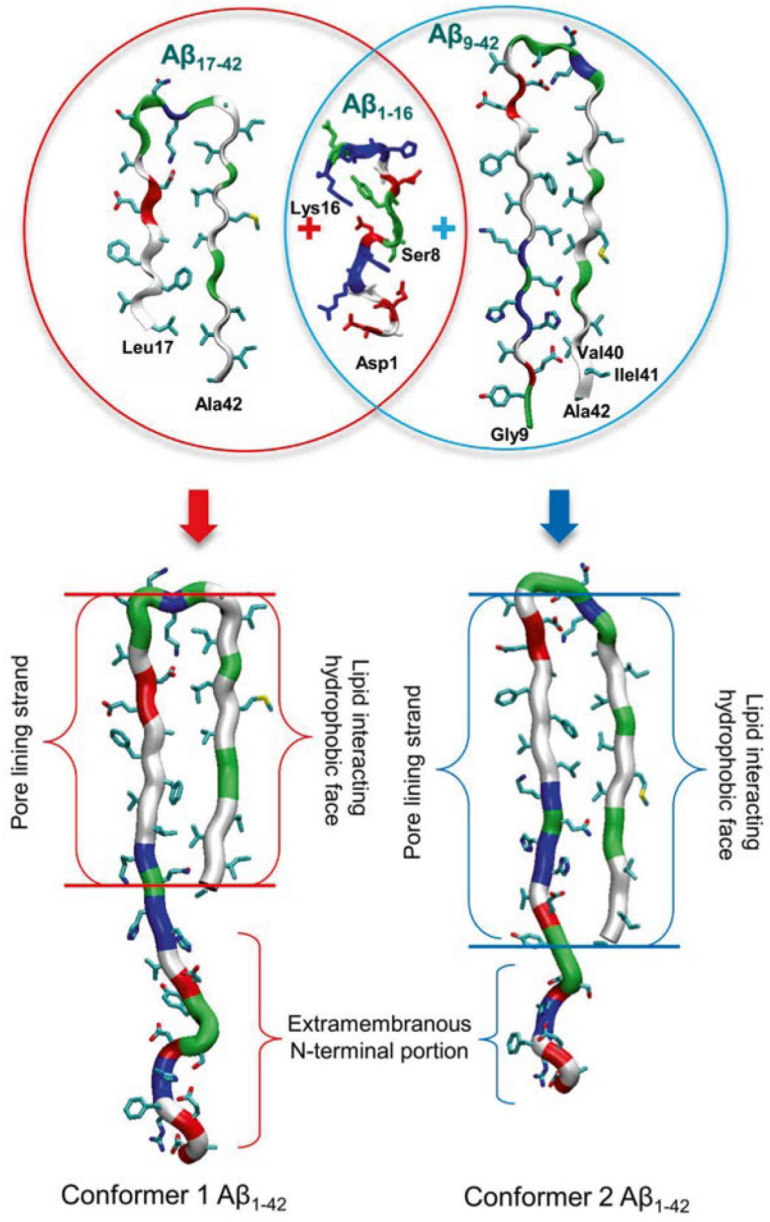

Fig. 3.

Schematic diagram for the constructions of full-length $A\beta_{1–42}$ peptides. The U-shaped Aβ monomers, $A\beta_{17–42}$ and $A\beta_{9–42}$, recover the missing N-terminal portions through the covalent connection with the solution structure of $A\beta_{1–16}$ (pdb code: 1ZE7), generating two $A\beta_{1–42}$ conformers (conformer 1 and 2) with different turns (from Jang et al. [8], reprinted with permission)

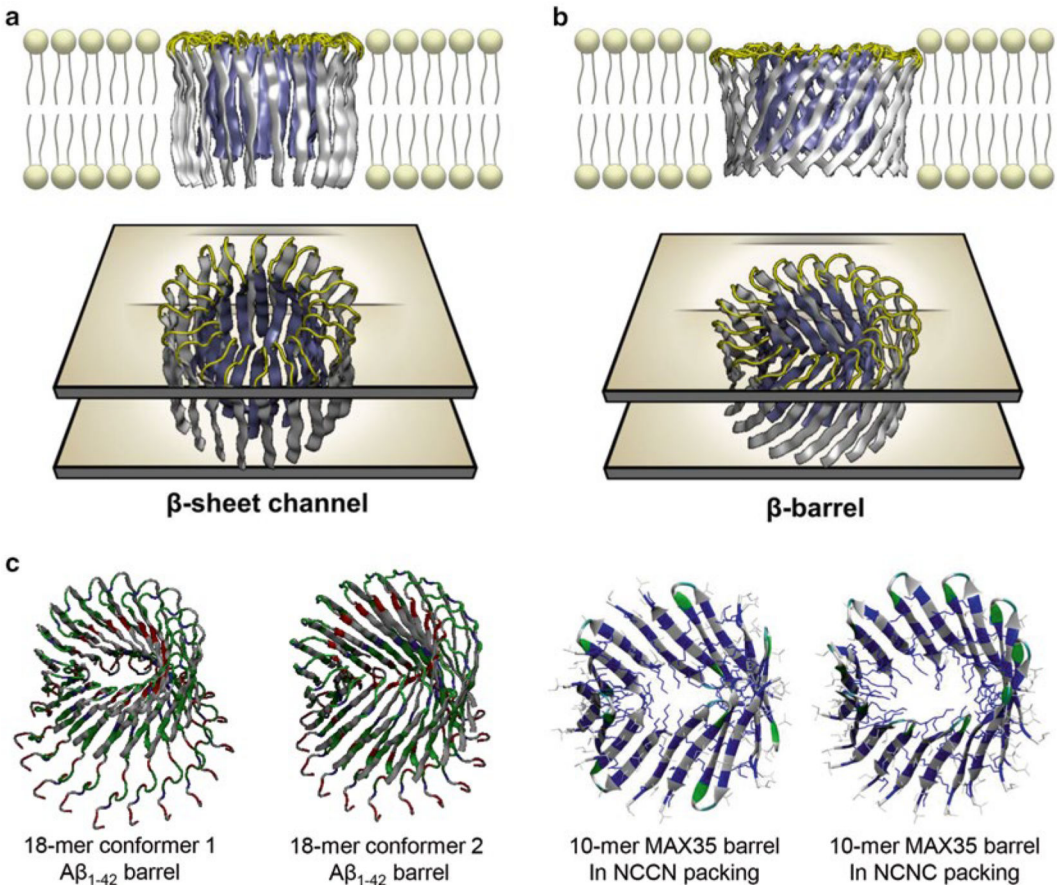

Fig. 4.

Constructing the conventional β-sheet channel and β-barrel in the membrane. (**a**) The conventional β-sheet channel has the β-strands that orient parallel to the membrane normal, (**b**) while the β-strands that orient obliquely to the membrane normal generate β-barrel structure (from Jang et al. [8], reprinted with permission). Both form a barrel-stave pore. (**c**) Examples are shown for the 18-mer conformer 1 and 2 $A\beta_{1–42}$ barrels, and 10-mer MAX35 barrels in NCCN and NCNC packing modes

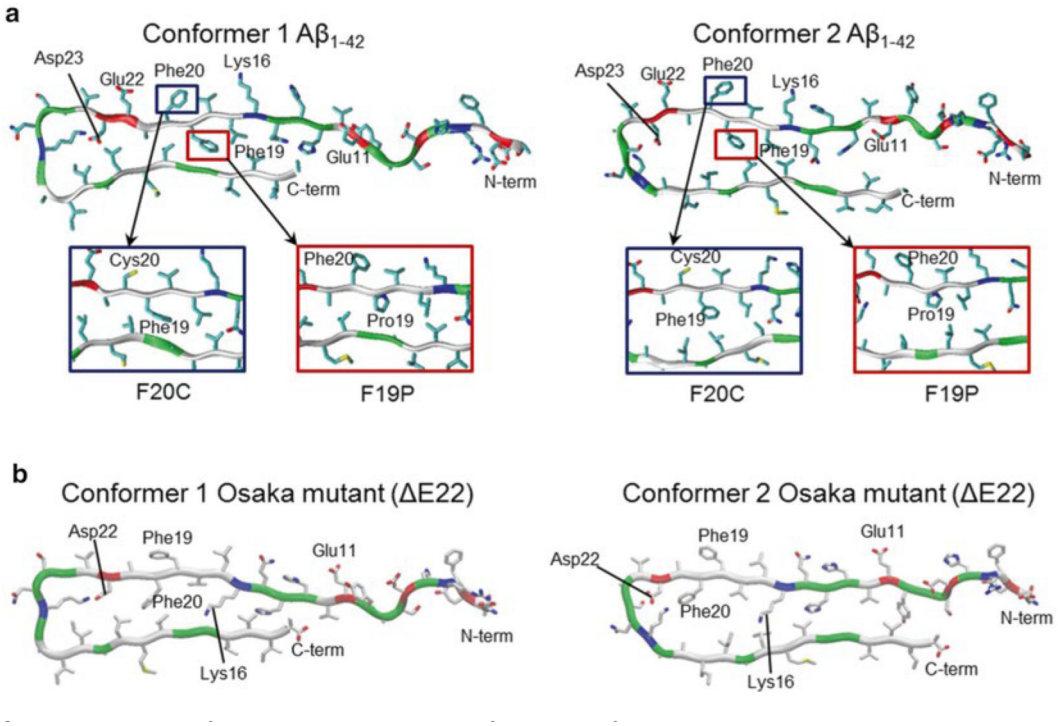

Fig. 5.

Aβ mutants conformations. (**a**) Monomer conformations of the $A\beta_{1–42}$ wild type (*top panels*) and F19P and F20C mutants (highlighted in *rectangular insets*) with two different conformers, conformer 1 (*left*) with turn at Ser26-Ile31 and conformer 2 (*right*) with turn at Asp23-Gly29. (**b**) Monomer conformations of the Osaka mutant (ΔE22) with two different conformers, conformer 1 (*left*) and conformer 2 (*right*). Several important residues in the pore-lining strand are marked. In the peptide ribbon, hydrophobic, polar/Gly, positively charged, and negatively charged residues are colored *white, green, blue*, and *red*, respectively

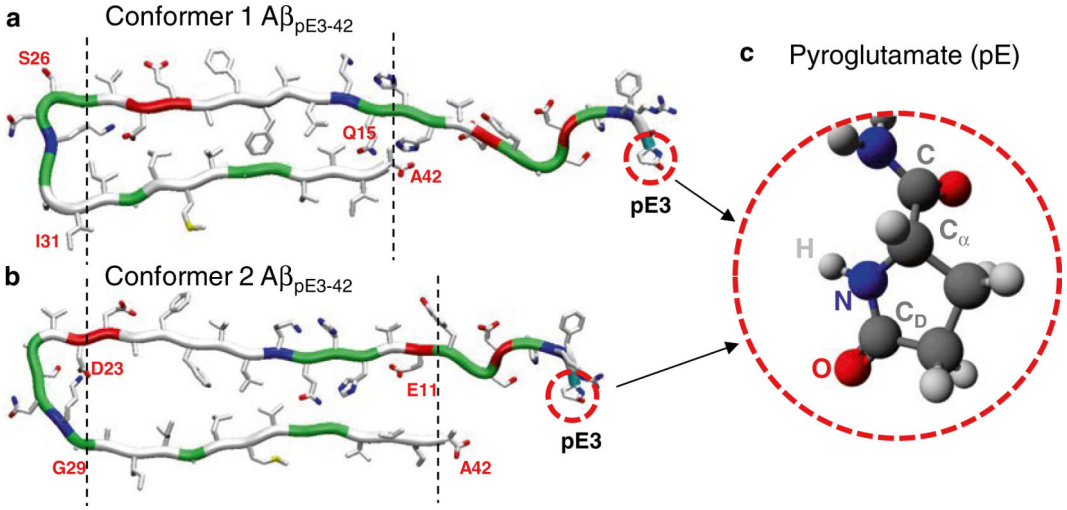

Fig. 6.

Conformations of pyroglutamate-modified Aβ ($Aβ_{pE}$) peptide. Monomer conformations of $Aβ_{pE3–42}$ with two different conformers, (**a**) conformer 1 with turn at Ser26-Ile31 and (**b**) conformer 2 with turn at Asp23-Gly29. (**c**) Molecular topology of the pyroglutamate at residue 3 (pE3). From Gilman et al. [42], reprinted with permission